npj | climate and atmospheric science

www.nature.com/npjclimatsci

ARTICLE OPEN

Check for updates

Locally opposite responses of the 2023 Beijing–Tianjin–Hebei extreme rainfall event to global anthropogenic warming

Dajun Zhao[1,2], Hongxiong Xu[1]✉, Ying Li[3]✉, Yubin Yu[4], Yihong Duan[1], Xiangde Xu[1] and Lianshou Chen[1]

The effect of anthropogenic warming on extreme rainfall events is a hot topic in this era of global warming, and increasing attention is being paid to its impact at regional and local scales. We explore the localized response of precipitation during the high-impact "23·7" extreme rainfall event in the Beijing–Tianjin–Hebei region under anthropogenic warming using ensemble convective-permitting simulations. We identify two sub-regions with opposite responses: anthropogenic warming decreased (increased) precipitation in the northern (southern) sub-region of the Beijing–Tianjin–Hebei area. Further analysis shows that anthropogenic warming intensified the remnant of Typhoon Dusuari and increased rainfall in its inner core but decreased rainfall in the peripheral spiral rain band. These are the main reasons for the locally inconsistent responses of extreme rainfall to anthropogenic warming. We emphasize that anthropogenic warming, as a global background signal, directly affects the intensity and structure of specific weather systems rather than local precipitation. A high-impact extreme rainfall event, therefore, cannot always be simply attributed to climate warming enhancing precipitation at every location in a particular region.

npj Climate and Atmospheric Science (2024)7:38 ; https://doi.org/10.1038/s41612-024-00584-7

INTRODUCTION

The Sixth Assessment Report of the Intergovernmental Panel on Climate Change (IPCC-AR6) anticipates that the occurrence and severity of heavy precipitation events are projected to escalate across the majority of terrestrial areas as a consequence of global climate change[1,2]. The influence of anthropogenic warming has increased the likelihood of extreme precipitation events by increasing the atmospheric moisture content[3]. This, in turn, will result in a more humid and fluctuating hydro-climate on timescales ranging from sub-daily to interannual[4–6]. Previous studies of extreme rainfall events have mainly focused on the characteristics and anomalies of the climatic background[7,8], synoptic impact weather systems[9–11], mesoscale convective systems[12], and cloud microphysical processes and the accompanying latent heating[13]. Overall, studies of multiple extreme rainfall events have shown that a single event often occurs in the context of favorable configurations of various weather systems and synergistic interactions across multiple scales[14–16].

Under the current global climate crisis, increasing attention is being paid to the detection and attribution of extreme rainfall events to anthropogenic climate change, including tropical cyclone precipitation (TCP) and tropical cyclone remote precipitation (TRP)[17–19]. Specifically, for TCP, the IPCC-AR6 report provides high confidence that event attribution studies of specific strong tropical cyclones have shown an increase in heavy precipitation due to anthropogenic effects[1]. Anthropogenic warming was recently found to have led to an increase in the regional rainfall in the July 2021 Henan extreme rainfall ("21·7" HNER), a catastrophic instance of TRP event, by about 7.5% (95% confidence interval 3.8–11%)[20]. Similar conclusions, but with a larger increase, were reached for the same event by other researchers[21]. This may be related to the different configurations in their convective-permitting simulations, which aim to explicitly resolve the intricate convective processes. There is a scientific consensus that extreme rainfall events are directly related to climate warming through basic thermodynamic principles, but complex dynamic processes also have an important role[22]. Clausius-Clapeyron (C-C) scaling can be deviated by changes in the large-scale atmospheric circulation and local weather patterns[23,24]. It has been shown that the area of extreme rainfall (≥500 mm) during the "21·7" HNER event increased by 29.9% (95% confidence interval 21–40%) as a result of anthropogenic warming and wetting, which caused stronger southerly winds[25]. These stronger winds led to stronger convergence in the lower troposphere and contributed to the increase in rainfall. It has been emphasized that shear convective organization was much more sensitive to large-scale dynamic forcing and resulted in more extreme precipitation in the "21·7" HNER event[26]. These studies have shed significant light on the attribution of extreme precipitation events on regional or local scales, laying a solid foundation for more in-depth research.

An extreme rainfall event occurred in the Beijing–Tianjin–Hebei (BTH) region in North China from 29 July to 1 August 2023, referred to as the "23·7" BTH extreme rainfall (BTHER) event. It was similar to the "21·7" HNER event, occurring in northern China during the rainy season[14]. Historically, droughts and floods frequently occur in the BTH region, where vulnerability and the risks from both weather and climate are high[16]. This region is characterized by sudden and localized heavy rainfall, which tends to be concentrated in a few rainy processes[14]. For instance, the "23·7" BTHER event was characterized by its long duration, the large amount of cumulative rainfall and historical extremes. The highest single-station cumulative precipitation recorded at Liangjiazhuang village in Hebei province surpassed 1003 mm within two days, which is more than twice the amount of precipitation typically received there in a whole year. Beijing recorded its heaviest precipitation since records began 140 years ago. The statistics also show that the intensity of the "23·7" BTHER

[1]State Key Laboratory of Severe Weather, Chinese Academy of Meteorological Sciences, Beijing 100081, China. [2]Shanghai Typhoon Institute, China Meteorological Administration, Shanghai 200030, China. [3]National Climate Centre, Beijing 100081, China. [4]China Meteorological Administration Training Centre, Beijing 100081, China.
✉email: xuhx@cma.gov.cn; yingli@cma.gov.cn

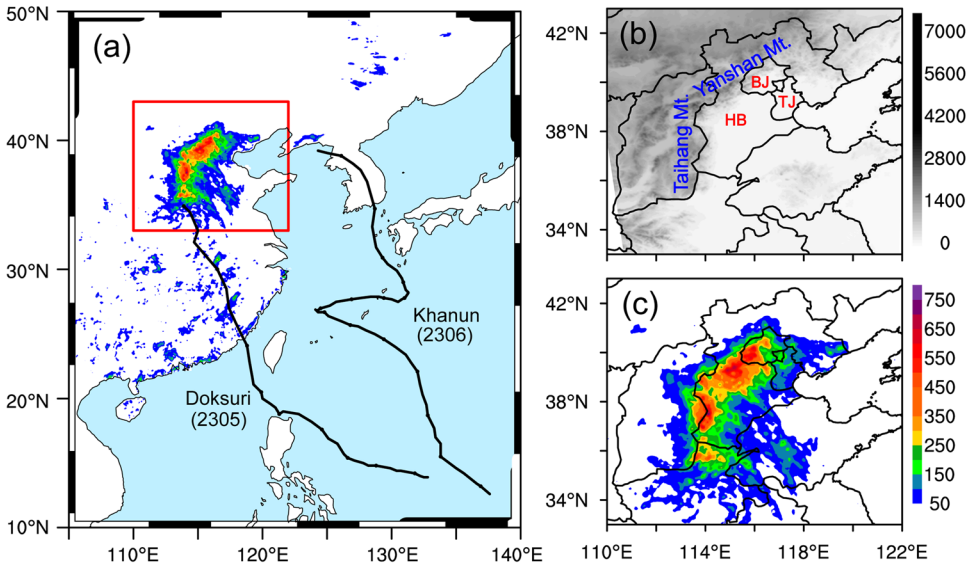

Fig. 1 Total observed precipitation and topographic features of the study region. a The 72-h accumulated rainfall (shading; units: mm) between 0000 UTC on 29 July 2023 and 0000 UTC on 1 August 2023 for the observed precipitation. The red box denotes our target region (33.0–43.0°N, 110.0–122.0°E) of Beijing–Tianjin–Hebei province and the black curves represent the tracks of Typhoon Doksuri (2305) and Typhoon Khanun (2306). **b** Topographic elevation (shading; units: m) within the target region showing the locations of the Taihang and Yanshan mountains (blue fonts) as well as the Beijing (BJ), Tianjin (TJ) and Hebei (HB) province (red fonts). **c** Zoomed-in distribution of the observed precipitation in the target region between 0000 UTC on 29 July 2023 and 0000 UTC on 1 August 2023 and the corresponding provincial boundaries.

event exceeded that of the most extreme rainstorm in the history of North China[27]. This rainfall and subsequent flooding resulted in a severe disaster in the BTH region, leading to considerable losses in terms of human life and property damage.

We carried out a timely and comprehensive analysis to investigate the impact of the dynamic and thermodynamic mechanisms of anthropogenic climate change on the intensity of the "23·7" BTHER event. In contrast with previous global or regional perspectives, we focus on smaller, local-scale responses. These findings will help us to better understand extreme rainfall events under the current global warming crisis.

RESULTS

Characteristics of the "23·7" BTHER event

Figure 1a shows the spatial distribution of the observed 72-h accumulated precipitation between 0000 UTC on 29 July 2023 and 0000 UTC on 1 August 2023. The rain bands to the south and north of 39°N in our target area had south–north and southwest–northeast orientations, respectively. This distribution pattern is consistent with the topographic orientations of the Taihang and Yanshan mountains, respectively (Fig. 1b). The cumulative rainfall in southwestern Beijing, central Hebei and Tianjin ranged from 350 to 550 mm, with some localities receiving >750 mm (Fig. 1c).

Three factors led to the formation of the "23·7" BTHER event. The first factor was abundant water vapor. The remnant of Typhoon Doksuri, still carrying abundant water vapor, converged with the southeasterly flow at the periphery of the subtropical high, which was also coupled with the remote delivery of water vapor from Typhoon Khanun. These three water vapor streams converged and led to the continuous transport of water vapor to the BTH region (Fig. 1a). The second factor was the occurrence of a blocking pattern caused by high-pressure systems. Specifically, the subtropical high was positioned to the east and the northern continental high to the north of the BTH region. These two high-pressure systems merged and formed a high-pressure dam, which blocked the forward movement of the typhoon remnant, leading to a long period of heavy rainfall (Figure not shown). The third factor contributing to the event was the orographic lift provided by the terrain. The Taihang and Yanshan mountains in the BTH region (Fig. 1c) uplifted and forced the condensation of the transported water vapor, increasing the intensity of the rainfall.

Ensemble convective-permitting simulations

Figure 2a–e provides a comprehensive comparative analysis of the simulated rainfall data from both the control (CTL) and natural (NAT) experiments with the observational data shown in Fig. 1c. The CTL simulation successfully captured the spatial distribution of the rain bands, particularly within the regions characterized by heavy rainfall (≥350 mm) across the BTH region (Fig. 2a). It effectively mirrored the observed spatial distribution of the rain bands, maintaining consistency with the orientation of the rain bands on the southern and northern sides of 39°N in our target area and exhibited a south–north and southwest–northeast orientation. Although there was a degree of overestimation in the CTL simulation, especially in the central-western region of Hebei province (~113.8°E, 38.0°N), it successfully reproduced the centers of extreme precipitation in the observational dataset. Notably, both Xingtai (114.5°E, 37.0°N) and southwestern Beijing showed centers of extreme precipitation (>750 mm), closely mirroring the observational data. The temporal aspect was similarly well replicated, with the simulated 3-h rainfall data closely paralleling the observations throughout the entire duration of the heavy rainfall event (Fig. 2e). In general, our CTL experiment reasonably reproduced the pattern and intensity of the rain bands and their evolution during the "23·7" BTHER event. Given this good alignment between the CTL simulation and the observational results, we used the D02 (3 km) model output to evaluate the impact of anthropogenic warming.

Compared with the CTL simulation, the NAT simulation exhibited a decrease in average precipitation across the target area, decreasing from 148.6 mm to 137.6 mm (Fig. 2b), constituting a decrease of ~7.5% (within a 95% confidence interval of 6.1–13.2%). Anthropogenic warming for this event was assessed to be between 0.6 and 0.8 °C (Fig. 2c), exceeding the thermodynamic anticipations derived exclusively from the Clausius-Clapeyron (C-C) relationship. This excess

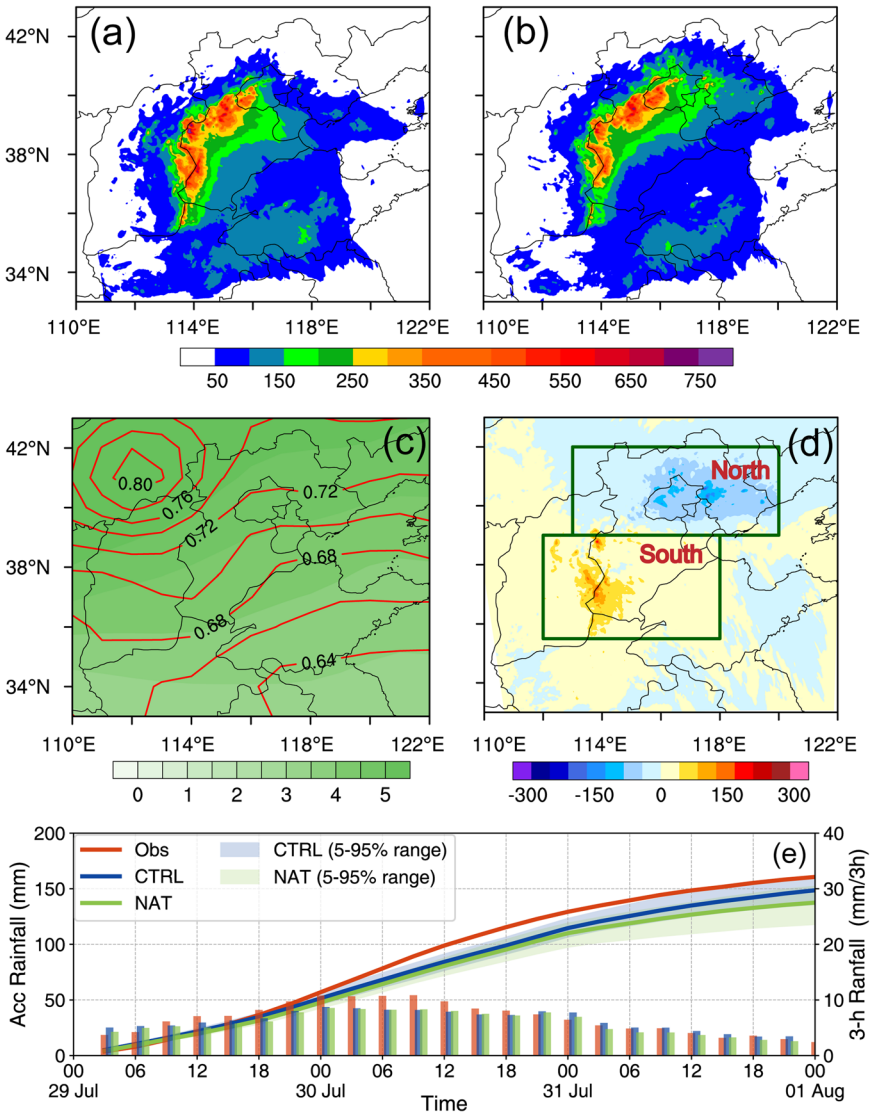

Fig. 2 Comparison of the simulated rainfall for the control and natural run experiments. The ensemble mean of the 72-h accumulated rainfall (shading; units: mm) for the **a** control (CTL) and **b** natural (NAT) sensitivity simulations between 0000 UTC on 29 July 2023 and 0000 UTC on 1 August 2023. **c** Anthropogenic warming and wetting indicated by the air temperature (contours, units: K) and specific humidity (shading, units: g kg^{-1}) averaged over 1000 hPa–700 hPa over the target region estimated by the CMIP6 selected model ensemble mean (historical run minus natural run) from 1984 to 2014. **d** The difference between **a** and **b**. The green boxes show the two sub-regions of opposite changes in cumulative precipitation in the north (39.0–42.0°N, 113.0–120.0°E) and south (35.5–39.0°N, 112.0–118.0°E). **d** Evolution of the regional average accumulated rainfall (curved lines; units: mm) and the 3-h rainfall (histograms; units: mm) for the observations (red), CTL simulation (blue) and NAT simulation (green) over the target region from 0000 UTC on 29 July 2023 to 0000 UTC on 1 August 2023. The corresponding ensemble member ranges are shaded for the CTL (light blue) and NAT (light green) simulations.

suggests the presence of other physical mechanisms, as corroborated by various earlier studies[20,21,26]. Fig. 2d further shows the difference in the 72-h accumulated precipitation between the CTL and NAT simulations. Interestingly, the total precipitation increased across most of the southern sub-region, whereas it decreased in most of the northern sub-region (Fig. 2d, green boxes). This indicates that the background anthropogenic warming increased rainfall in the southern sub-region, but decreased rainfall in the northern sub-region. Fig. 1b shows that the southern and northern sub-regions correspond to the Taihang and Yanshan mountains, respectively.

Understanding the changes in extreme events in a warming world requires an understanding of changes in the atmospheric circulation besides thermodynamics[28]. The remnant of Typhoon Dusuari was the primary influencing weather system for the "23·7" BTHER event. Given that we recognize the primary driver of this precipitation event as typhoon circulation, a pertinent question arises: could global warming potentially influence extreme rainfall by altering the dynamics of typhoon circulation?

Impact of anthropogenic warming on the remnant of Typhoon Doksuri

We now focus on analyzing how anthropogenic warming affected the remnant of Typhoon Dusuari and its consequent effects on the divergent precipitation response patterns in the northern and southern sub-regions. Fig. 3a, b shows the evolution of the track and intensity of the remnant of Typhoon Doksuri simulated in the CTL and NAT experiments, respectively. The results show that anthropogenic warming resulted in a smaller overall change in the track of the remnant of Typhoon Doksuri, which was slightly to the west and south (Fig. 3a). We believe that this change had a limited impact on the distribution of precipitation in the two sub-regions.

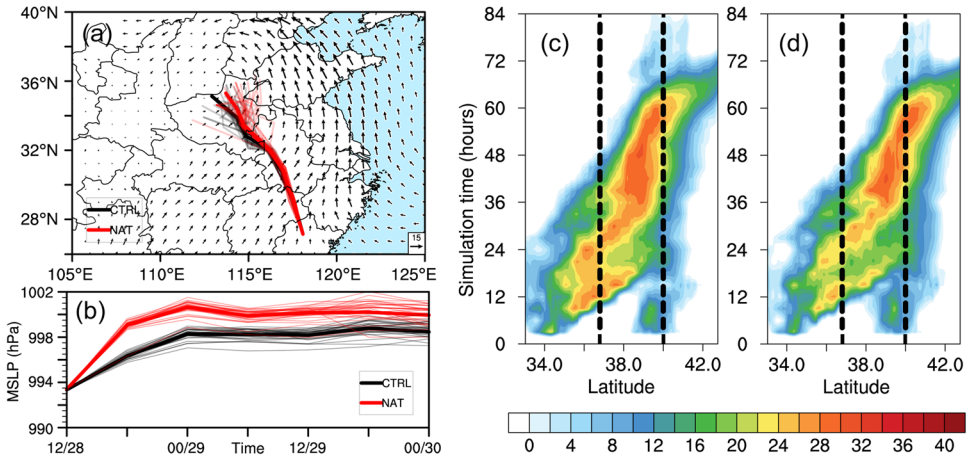

Fig. 3 Evolutionary characteristics of the remnant of Typhoon Doksuri. a Track of the remnant of Typhoon Doksuri as simulated in the CTL (black lines) and NAT (red lines) experiments, with the overlay representing the daily average horizontal wind vectors at 850 hPa for the CTL experiment on 30 July 2023. The thick lines denote the tracks from the ensemble mean, whereas the thin lines represent those of the ensemble members. **b** The intensity (hPa) of the remnant of Typhoon Doksuri for the CTL (black lines) and NAT (red lines) simulations, where the thick and thin lines represent the intensities derived from the ensemble mean and the ensemble members, respectively. The time–latitude Hovmöller diagrams of the average maximum radar reflectivity (units: dBZ) over the region 110.0–122.0°E for the **c** CTL and **d** NAT simulations. The dashed black reference lines along 36.8°N and 40.0°N are representative locations in the southern and northern sub-regions, respectively, shown in Fig. 2d.

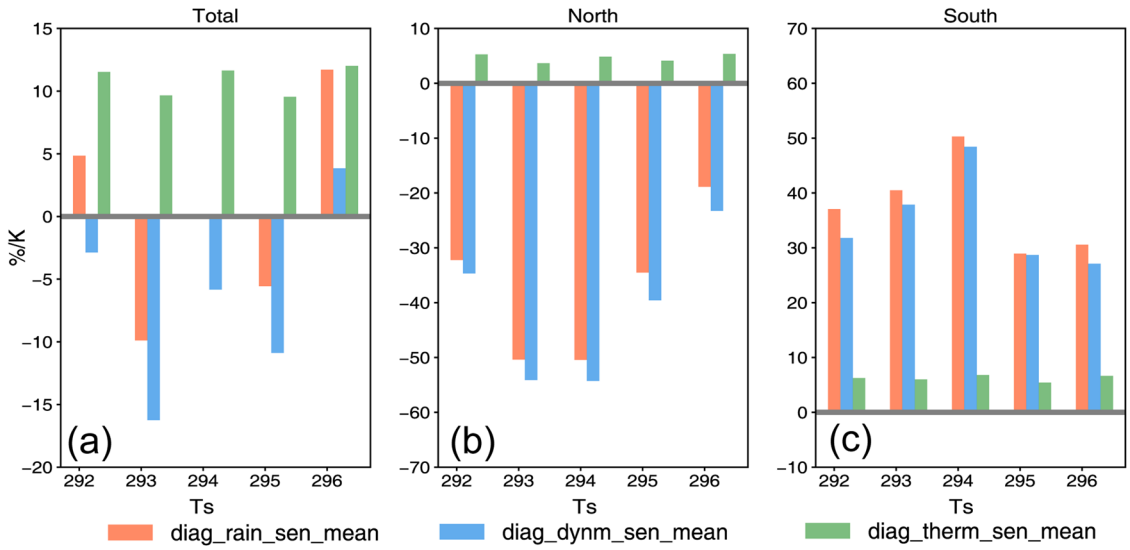

Fig. 4 Sensitivity of the extreme precipitation to anthropogenic warming and the thermodynamic and dynamic components. Averaged 72-h extreme precipitation sensitivity (orange bars; units: % K^{-1}) and its associated dynamic (blue bars; units: % K^{-1}) and thermodynamic (green bars; units: % K^{-1}) components in relation to changes in surface temperature due to anthropogenic warming (units: K) for the average of **a** the two sub-regions, **b** the northern sub-region, and **c** the southern sub-region.

However, the effect of anthropogenic warming on the intensity of the remnant of Typhoon Doksuri was much more significant, making it stronger, as seen by the minimum sea-level pressure in Fig. 3b.

The time–latitude Hovmöller diagrams of the average maximum radar reflectivity (Fig. 3c, d) clearly show that anthropogenic warming had a large impact on the convective evolutionary characteristics of the remnant of Typhoon Doksuri and that this impact was closely related to the distribution of precipitation in the two sub-regions. A comparison of two representative stations in the northern and southern sub-regions (reference lines in Fig. 3c, d) shows that anthropogenic warming strengthened (weakened) convection in the southern (northern) sub-region. This is consistent with the response of the precipitation in southern and northern sub-regions (Fig. 2d). The following analysis focuses on the physical mechanisms responsible for these opposite responses.

Possible mechanisms of locally opposite responses

We decomposed the changes in precipitation extremes into contributions from thermodynamic and dynamic factors using a robust physical scaling diagnostic technique[29–31] for aggregated changes in extreme precipitation. Fig. 4 shows the sensitivity of the extreme precipitation to anthropogenic warming as indicated by the changes in surface temperature and its thermodynamic and dynamic components. The contributions of the dynamic and thermodynamic terms to the diagnostic sensitivity of the extreme precipitation are opposite for the average of the two sub-regions (Fig. 4a). Their difference in magnitude is not significant, so it is

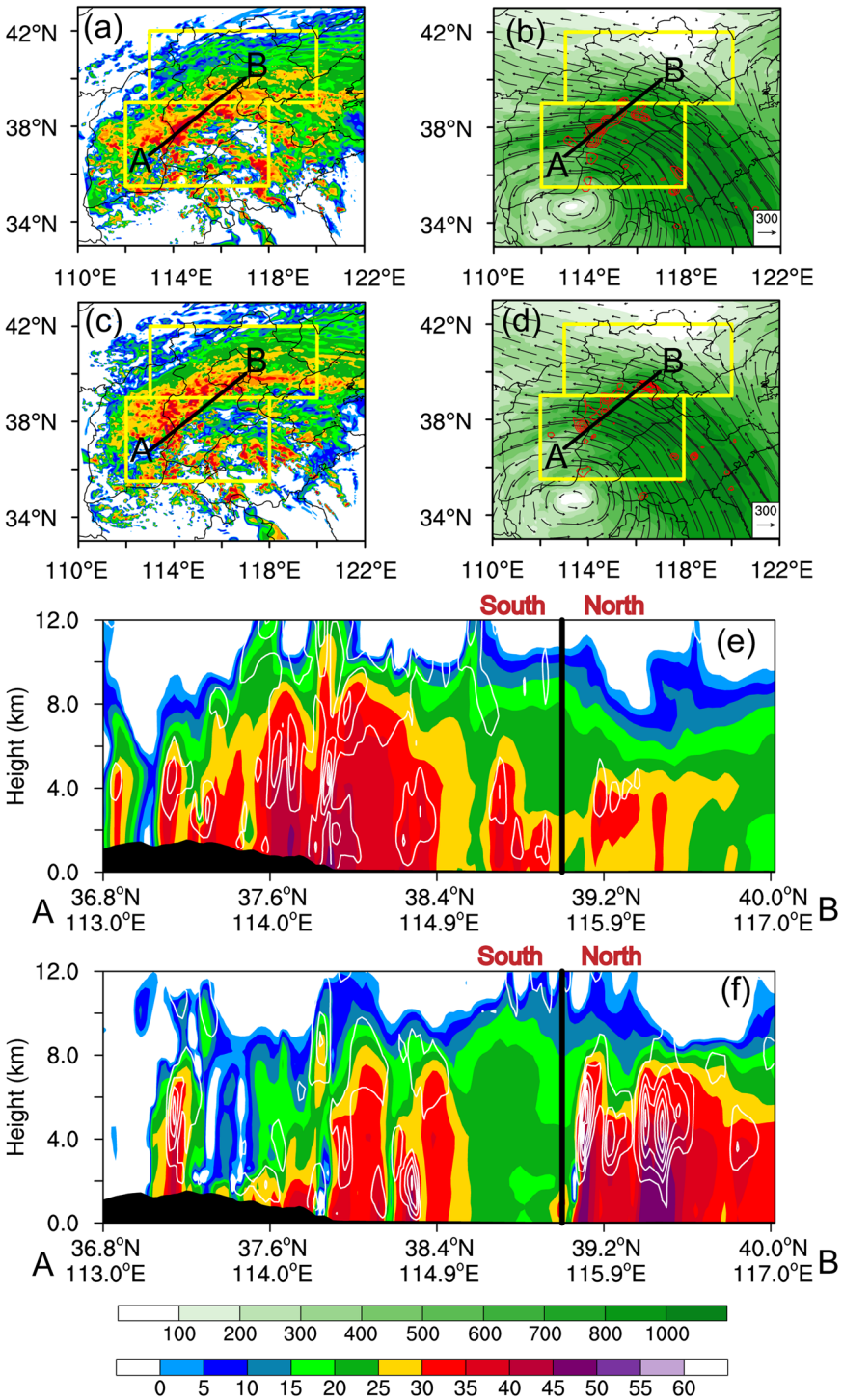

Fig. 5 The different convective organizational features in different sub-regions associated with the anthropogenic warming. Plan view of the maximum radar reflectivity (**a**) (shading; units: dBZ) and column-integrated moisture flux (vectors), its magnitude (shaded, unit: kg m^{-1} s^{-1}) and its convergence (**b**) (contour, unit: 10^{-5} g kg^{-1} s^{-1}) for the CTL and NAT (**c**, **d**) simulations at 0000 UTC on 30 July 2023. The yellow boxes in **a**–**d** are the same as in Fig. 2d. The vertical cross-sections along line A–B of the maximum radar reflectivity (shading; units: dBZ) overlain with the vertical velocity (contours; units: m s^{-1}) for the **e** CTL and **f** NAT experiments. The topography is shaded in black, and the bold black lines in **e** and **f** indicate the dividing line between the northern and southern sub-regions.

difficult to conclude which one is dominant. Interestingly, when we look at the northern and southern sub-regions separately (Fig. 4b, c), we see that, although the contribution of the thermodynamic component is roughly equal in both sub-regions and increases the amount of extreme precipitation, it is the dynamic component that truly dominates the event. In other words, the locally opposite responses of the two sub-regions as a result of anthropogenic warming are both dominated by the dynamic component.

Figure 5a–f shows the convective organizational features as well as the deep layer moisture and circulation configurations in the different sub-regions for the CTL and NAT experiments. Upon

comparing Fig. 5a and c, it is evident that in the context of anthropogenic warming, convective activity intensified in the southern sub-region while it was mitigated in the northern sub-region. Similarly, a comparison between Fig. 5b and d indicates an enhanced moisture flux and convergence in the southern sub-region, contrasting with a reduced presence in the northern sub-region. The delineated shift is clearly evident along the reference lines A–B. The vertical cross-section along A–B (Fig. 5e, f) shows that the intense convective zone (≥30 dBZ) in the southern sub-region not only expands in horizontal area, but also has an increased vertical extent under conditions of anthropogenic warming. This is particularly pronounced near the Taihang Mountains and is coupled with more robust upward vertical movement and horizontal moisture convergence. By contrast, convective activity and vertical motion in the northern sub-region show a marked reduction under the influence of anthropogenic warming. This aligns with the enhanced remnants of Typhoon Doksuri attributed to anthropogenic warming, as discussed in the previous section (Fig. 3b). Such a trend correlates with the increase (decrease) in convective activity within the inner core (periphery) region of the remnant of Typhoon Doksuri.

DISCUSSION

We analyzed the impact of anthropogenic warming on the "23·7" BTHER event using large ensemble CTL and NAT convective-permitting simulations under the conditional extreme event attribution framework. In contrast to the commonly observed trend of continuous increase in extreme rainfall events at global or national scales[32], our study narrowed the lens to finer spatial resolutions similar to administrative division scales[33]. Our results reveal that anthropogenic warming has increased the regional averaged precipitation within the whole target region, which is in line with our previous results on the"21·7" HNER[25]. However, more notably, here we identified two sub-regions exhibiting contrasting local responses. In detail, the two sets of experiments showed that the 72-h averaged precipitation increased by 22.0% (95% confidence interval 11.7–28.0%) in the southern sub-region (~2300 km^2 and including Beijing, Tianjin, northern Shanxi and northern Hebei), but decreased by −34.2% (95% confidence interval −117 to −21.3%) in the northern sub-region (~2300 km^2 and including southern Shanxi and southern Hebei) under anthropogenic warming. Intriguingly, both these variations surpassed the anticipatory projections deduced from the C-C relationship. Delving deeper via robust physical scaling diagnostics, it became evident that dynamic processes predominantly drove the patterns of extreme precipitation in these two sub-regions.

Turning our attention to the dominant synoptic system influencing the "23·7" BTHER event, specifically the delineated weather patterns[22,24], we scrutinized the remnant of Typhoon Doksuri. Our findings suggest that anthropogenic warming not only subtly altered the track of the remnant of Typhoon Doksuri, but also markedly amplified its intensity. This intensified remnant displayed pronounced vertical motion and convection within its inner core region, which corresponded to our southern sub-region. By contrast, its periphery (aligned with our northern sub-region) showed subdued vertical motion and convection. In addition, the north–south alignment of the Taihang Mountains lies perpendicular to the low-level easterly flow from the remnant of Typhoon Doksuri, further enhancing convection and precipitation within its inner core region. Synthesizing these insights, we posit that the interplay between the local topography and anthropogenic warming directly affected the intensity and structure of the remnant of Typhoon Doksuri and shaped the locally opposite response patterns of precipitation. Actually, climate projections have indicated a wetting trend over high mountain Asia in the future[34–36], and the extreme precipitation is also projected to increase in major mountainous regions[1], our findings highlight the importance of considering the impact of local topography when we conduct similar attribution studies in the future.

It is important to emphasize that the findings of this study do not negate the conclusions of earlier attribution studies[25,37], but serve as a valuable extension. Although there is a prevailing consensus that global anthropogenic warming is intensifying extreme precipitation[1,38], and has notably reshaped the patterns of typhoon-induced heavy rainfall[39] and the intensity of rainfall rates[40,41], it is crucial to avoid over-generalizing. Specifically, it is inappropriate to assert that anthropogenic warming makes precipitation stronger everywhere in a local area during a single extreme rainfall event, as illustrated by the cities of Beijing and Tianjin during the "23·7" BTHER event. Our study effectively addresses the impact of global warming on extreme precipitation events by distinguishing between global and local influences. This distinction is essential for shaping policies and strategies, and it allows us to combine global actions like reducing emissions with local preparations such as improving drainage systems and early warning systems. Overall, our research provides practical insights that enable informed decision-making and enhance resilience in the face of extreme precipitation events. It serves as a bridge between global climate concerns and local disaster management.

METHODS

Model configurations

We used the Weather Research and Forecasting (WRF) model Version 4.4.3 to investigate the impact of anthropogenic climate change on the "23·7" BTHER event[42]. The initial and lateral boundary conditions were derived from the European Centre for Medium-Range Weather Forecasts fifth-generation global reanalysis (ERA5) hourly dataset with a horizontal resolution of 0.25° and 50 vertical levels[43]. The model top was set at 50 hPa. We used 84-h simulations with double two-way interactive nested domains (D01 and D02) with horizontal resolutions of 12 and 3 km and (652 × 463) and (345 × 385) corresponding grid points, respectively. The simulation was initialized at 1200 UTC on 28 July 2023 with the outer domain (D01) centred at (25.0°N, 120.0°E). This domain was concentrated in the BTH region and covered the development, enhancement and subsequent weakening stages of the "23·7" BTHER event. The physical parameterization schemes of the WRF model include the aerosol-aware Thompson microphysics scheme[44], the rapid radiative transfer model for the global climate scheme for long- and shortwave radiative flux calculations[45], the Mellor–Yamada–Nakanishi–Niino scheme for the planetary boundary layer and the surface layer[46], and the unified Noah land surface model[47]. The Kain–Fritsch cumulus parameterization scheme[48] is used for D01, which is not used in the inner domain D02.

Pseudo-global warming (PGW) experiment

Following previous studies[25,49–51], we adopted the internationally recognized PGW approach to quantitatively evaluate the thermodynamic aspects of anthropogenic climate change. A companion sensitivity simulation (the NAT simulation) was conducted with the same parameter configurations as the CTL simulation, but with the addition of an "increment" to the initial and boundary conditions for the CTL simulation. The specific value of this increment was derived from the ensemble mean differences of ten global climate models (Table 1) participating in the Coupled Model Intercomparison Project Phase 6 between the all-forcing historical run and its natural-only forcing counterpart during 1984–2014.

The CTL and NAT simulations only differed in the thermodynamic components of the initial and boundary conditions; they retained the same dynamic components. The differences between

Table 1. The ten global models used for the estimation of anthropogenic warming.

Model name	Organization	Country
ACCESS-CM2	ACCESS	Australia
ACCESS-ESM1-5	ACCESS	Norway
BCC-CSM2-MR	BCC	China
CanESM5	CCCma	Canada
CESM2	NCAR	USA
FGOALS-g3	IAP	China
GFDL-CM4	GFDL	USA
IPSL-CM6A-LR	IPSL	France
MIROC6	MIROC	Japan
MRI-ESM2-0	MRI	Japan

the simulations could, therefore, be attributed to anthropogenic climate change. The bias in the individual climate models and variations in the decadal timescale were reduced by using the model ensemble mean and the long-term mean. To avoid any further uncertainty arising from unresolved processes and their interactions at the sub-grid scale in convective-permitting simulations, we also performed 30-member ensemble simulations using the stochastic kinetic energy backscatter scheme for both the CTL and NAT experiments. The resulting uncertainties were then quantified using the 30 members of each experiment in the subsequent analysis.

Robust physical scaling

Following the previous studies[28–31], the robust physical scaling diagnostic for precipitation extremes can be simplified as:

$$P_e \approx -\left\{\omega_e \frac{dq_s}{dp}\bigg|_{\theta^*}\right\} \quad (1)$$

Where ω_e represents the vertical velocity, q_s is the saturation specific humidity, θ^* is the saturation equivalent potential temperature, $\{\cdot\}$ denotes a mass-weighted integration from 1000 hPa to 50 hPa. In Eq. (1), ω_e is referred to as the dynamic component which affects the magnitude of the condensation rate during the rainfall process, and $\frac{dq_s}{dp}\big|_{\theta^*}$ is defined as the thermodynamic component which shows the derivative of the q_s along a moist adiabat with the constant θ^*. Following the methodology outlined in Qin et al.[26], this study employs the CTL and NAT simulations to systematically quantify the sensitivity of extreme precipitation across discrete 1 K surface temperature intervals, as illustrated in Fig. 4.

Data

Three-hourly cumulative multisource integrated precipitation data (0.1° × 0.1°), provided by the National Meteorological Information Center of the China Meteorological Administration (NMIC/CMA), were used as the observational precipitation. These data were merged, with strict quality control procedures, from rain gauge measurements at >30,000 automatic weather stations in China in conjunction with the Climate Precipitation Center Morphing precipitation product[52]. The track and intensity data of typhoons were collected from the official typhoon bulletins issued by the CMA. The remnant of Typhoon Doksuri was tracked via its minimum pressure at sea level.

We focused on the 72-h period between 0000 UTC on 29 July 2023 and 0000 UTC on August 1, 2023, which covers the record-breaking precipitation in both the northern and southern sub-regions of interest. The targeted region was (33.0–43.0°N, 110.0–122.0°E), much smaller than the D02 model domain. This ensured the results of the analysis were minimally affected by the model domain boundaries.

DATA AVAILABILITY

The ERA5 data are downloaded from the Climate Data Store https://doi.org/10.24381/cds.bd0915c6, and the CMIP6 data is obtained from https://esgf-node.llnl.gov/search/cmip6/. In compliance with data policies in China, the precipitation datasets employed in this study are not publicly available online. For detailed information regarding data access, researchers and interested parties are encouraged to contact either the China Meteorological Data Service Center (http://data.cma.cn/en) or the China Meteorological Administration (CMA) (http://www.cma.gov.cn/en2014/aboutcma/contactus/).

CODE AVAILABILITY

The figures in this study were all plotted using the NCAR Command Language (NCL), as detailed in https://www.ncl.ucar.edu/Applications/. All codes are also available from the corresponding author upon reasonable request.

Received: 28 October 2023; Accepted: 22 January 2024;
Published online: 06 February 2024

REFERENCES

1. IPCC. Climate Change 2021: The Physical Science Basis. Contribution of Working Group I to the Sixth Assessment Report of the Intergovernmental Panel on Climate Change (Cambridge University Press, 2021).
2. Qian, C., Ye, Y. B., Chen, Y. & Zhai, P. M. An updated review of event attribution approaches. *J. Meteorol. Res.* **36**, 227–238 (2022).
3. Zhou, T., Ren, L. & Zhang, W. Anthropogenic influence on extreme Meiyu rainfall in 2020 and its future risk. *Sci. China Earth Sci.* **64**, 1633–1644 (2021).
4. Fowler, H. J. et al. Anthropogenic intensification of short-duration rainfall extremes. *Nat. Rev. Earth Environ.* **2**, 107–122 (2021).
5. Zhang, W. et al. Increasing precipitation variability on daily-to-multiyear timescales in a warmer world. *Sci. Adv.* **7**, eabf8021 (2021).
6. Zhang, W. et al. Constraining extreme precipitation projections using past precipitation variability. *Nat. Commun.* **13**, 6319 (2022).
7. Li, Y. & Zhao, D. J. Climatology of tropical cyclone extreme rainfall over China from 1960 to 2019. *Adv. Atmos. Sci.* **39**, 320–332 (2022).
8. Zhao, D. J., Gao, W. H., Xu, H. X., Yu, Y. B. & Chen, L. S. A modeling study of cloud physical properties of extreme and non-extreme precipitation in landfalling typhoons over China. *Atmos. Res.* **277**, 106311 (2022).
9. Zhao, D. J., Yu, Y. B. & Chen, L. S. Impact of the monsoonal surge on extreme rainfall of landfalling tropical cyclones. *Adv. Atmos. Sci.* **38**, 771–784 (2021).
10. Xu, H., Duan, Y. & Xu, X. Indirect effects of binary typhoons on an extreme rainfall event in Henan province, China from 19 to 21 July 2021: 1. Ensemble-based analysis. *J. Geophys. Res. Atmos.* **127**, e2021JD036265 (2022).
11. Xu, H. et al. Indirect effects of binary typhoons on an extreme rainfall event in Henan Province, China from 19 to 21 July 2021: 2. Numerical study. *J. Geophys. Res. Atmos.* **127**, e2021JD036083 (2022).
12. Yin, J. F. et al. A possible dynamic mechanism for rapid production of the extreme hourly rainfall in Zhengzhou City on 20 July 2021. *J. Meteorol. Res.* **36**, 6–25 (2022).
13. Xu, H. et al. Indirect effects of binary typhoons on an extreme rainfall event in Henan province, China from 19 to 21 July 2021: 3. Sensitivities to microphysics schemes. *J. Geophys. Res. Atmos.* **128**, e2022JD037936 (2023).
14. Tao, S. Y. Rainstorms in China, pp 225 (Science Press, 1980) [in Chinese].
15. Meng, Z. et al. Review of Chinese atmospheric science research over the past 70 years: synoptic meteorology. *Sci. China Earth Sci.* **62**, 1946–1991 (2019).
16. Ding, Y. H., Liu, Y. J. & Song, Y. F. East Asian summer monsoon moisture transport belt and its impact on heavy rainfalls and floods in China. *Adv. Water Sci.* **31**, 629–643 (2020).
17. National Academies of Sciences, Engineering, and Medicine. Attribution of Extreme Weather Events in the Context of Climate Change (The National Academies Press, 2016).
18. Zhai, P. M., Zhou, B. Q. & Chen, Y. A review of climate change attribution studies. *J. Meteorol. Res.* **32**, 671–692 (2018).
19. Zhang, W. et al. Urbanization exacerbated the rainfall and flooding caused by hurricane Harvey in Houston. *Nature* **563**, 384–388 (2018).
20. Wang, J., Chen, Y. & Nie, J. On the role of anthropogenic warming and wetting in the July 2021 Henan record-shattering rainfall. *Sci. Bull. (Beijing)* **67**, 2055–2059 (2022).

21. Ma, Y. et al. Anthropogenic climate change enhances the July 2021 super-heavy rainfall event in Central China. *Bull. Am. Meteorol. Soc.* **104**, E736–E741 (2023).
22. King, A. D., Reid, K. J. & Saunders, K. R. Communicating the link between climate change and extreme rain events. *Nat. Geosci.* **16**, 552–554 (2023).
23. Wu, L. G., Zhao, H. K., Wang, C., Cao, J. & Liang, J. Understanding of the effect of climate change on tropical cyclone intensity: a review. *Adv. Atmos. Sci.* **39**, 205–221 (2022).
24. Gu, L. et al. Large anomalies in future extreme precipitation sensitivity driven by atmospheric dynamics. *Nat. Commun.* **14**, 3197 (2023).
25. Zhao, D. J. et al. Quantitative attribution of historical anthropogenic warming on the extreme rainfall event over Henan in July 2021. *Environ. Res. Lett.* **18**, 104037 (2023).
26. Qin, H. et al. Climate change attribution of the 2021 Henan extreme precipitation: impacts of convective organization. *Sci. China Earth Sci.* **65**, 1837–1846 (2022).
27. Fu, J. L. et al. Preliminary study on the refined characteristics of rainfall intensity and dynamic and thermodynamic conditions in the July 2023 severe torrential rain in North China. *Meteor Mon.* **49**, 1435–1450 (2023).
28. Otto, F. et al. The attribution question. *Nat. Clim. Change* **6**, 813–816 (2016).
29. Pfahl, S., O'Gorman, P. & Fischer, E. Understanding the regional pattern of projected future changes in extreme precipitation. *Nat. Clim. Change* **7**, 423–427 (2017).
30. Dai, P. & Nie, J. What controls the interannual variability of extreme precipitation? *Geophys. Res. Lett.* **48**, e2021GL095503 (2021). (2021).
31. Huang, Z., Tan, X., Gan, T. Y., Liu, B. & Chen, X. Thermodynamically enhanced precipitation extremes due to counterbalancing influences of anthropogenic greenhouse gases and aerosols. *Nat. Water* **1**, 614–625 (2023).
32. Camargo, S. J. et al. An update on the influence of natural climate variability and anthropogenic climate change on tropical cyclones. *Trop. Cyclone Res. Rev.* **12**, 216–239 (available online 13 October 2023).
33. Stott, P. A. et al. Detection and attribution of climate change: a regional perspective. *WIREs Clim. Change* **1**, 192–211 (2010).
34. Lalande, M., Ménégoz, M., Krinner, G., Naegeli, K. & Wunderle, S. Climate change in the High Mountain Asia in CMIP6. *Earth Syst. Dyn.* **12**, 1061–1098 (2021).
35. Yao, T. et al. The imbalance of the Asian water tower. *Nat. Rev. Earth Environ.* **3**, 618–632 (2022).
36. Jiang, J. et al. Precipitation regime changes in High Mountain Asia driven by cleaner air. *Nature* **623**, 544–549 (2023).
37. Kanada, S., Tsuboki, K., Aiki, H., Tsujino, S. & Takayabu, I. Future enhancement of heavy rainfall events associated with a typhoon in the midlatitude regions. *SOLA* **13**, 246–251 (2017).
38. Trenberth, K. E., Dai, A., Rasmussen, R. M. & Parsons, D. B. The changing character of precipitation. *Bull. Am. Meteorol. Soc.* **84**, 1205–1217 (2003).
39. Utsumi, N. & Kim, H. Observed influence of anthropogenic climate change on tropical cyclone heavy rainfall. *Nat. Clim. Change* **12**, 436–440 (2022).
40. Liu, M. et al. Causes of large projected increases in hurricane precipitation rates with global warming. *npj Clim. Atmos. Sci.* **2**, 38 (2019).
41. Wang, C. et al. How much of Typhoon Morakot's extreme rainfall is attributable to anthropogenic climate change? *Int. J. Climatol.* **39**, 3454–3464 (2019).
42. Skamarock, W. C. et al. A description of the advanced research WRF model version 4. *NCAR Technical Notes NCAR/TN-556+STR*, https://doi.org/10.5065/1dfh-6p97 (2019).
43. Hersbach, H. et al. The ERA5 global reanalysis. *Q. J. R. Meteorol. Soc.* **146**, 1999–2049 (2020). 2020.
44. Thompson, G. & Eidhammer, T. A study of aerosol impacts on clouds and precipitation development in a large winter cyclone. *J. Atmos. Sci.* **71**, 3636–3658 (2014).
45. Iacono, M. J. et al. Radiative forcing by long–lived greenhouse gases: calculations with the AER radiative transfer models. *J. Geophys. Res.* **113**, D13103 (2008).
46. Janjić, Z. I. The step-mountain eta coordinate model: further developments of the convection, viscous sublayer, and turbulence closure schemes. *Mon. Weather Rev.* **122**, 927–945 (1994).
47. Tewari, M. F. et al. Implementation and verification of the unified NOAH land surface model in the WRF model. *In:* Proceedings of the 20th Conference on Weather Analysis and Forecasting/16th Conference on Numerical Weather Prediction, 11–15 (American Meteorological Society, 2004).
48. Kain, J. S. The Kain–Fritsch convective parameterization: an update. *J. Appl. Meteorol.* **43**, 170–181 (2004).
49. Shepherd, T. G. A common framework for approaches to extreme event attribution. *Curr. Clim. Change Rep.* **2**, 28–38 (2016).
50. Patricola, C. M. & Wehner, M. F. Anthropogenic influences on major tropical cyclone events. *Nature* **563**, 339–346 (2018).
51. Michaelis, A. C., Lackmann, G. M. & Robinson, W. A. Evaluation of a unique approach to high-resolution climate modeling using the model for prediction across scales-atmosphere (MPAS-A) version 5.1. *Geosci. Model Dev.* **12**, 3725–3743 (2019).
52. Shen, Y., Zhao, P. & Pan, Y. A high spatiotemporal gauge-satellite merged precipitation analysis over China. *J. Geophys. Res. Atmos.* **119**, 3063–3075 (2014).

ACKNOWLEDGEMENTS

The authors are grateful to the editor and three anonymous reviewers for their constructive comments in improving the quality of this study. This work was supported by the National Key R&D Program of China (2023YFC3008501, 2023YFC3008005), National Natural Science Foundation of China (42192554, 42375015, 42375014), Shanghai Typhoon Research Foundation (TFJJ202201), the Basic Research Fund of CAMS (2023Z020), Typhoon Scientific and Technological Innovation Group of China Meteorological Administration (CMA2023ZD06), Financial Meteorology Innovation Group of China Meteorological Administration (CMA2024ZD03) and Open Grants of the State Key Laboratory of Severe Weather (2023LASW-B10). We acknowledge the World Climate Research Program, which, through its Working Group on Coupled Modeling, coordinated and promoted CMIP6.

AUTHOR CONTRIBUTIONS

D.Z., H.X. and Y.L. designed the research; D.Z. and H.X. performed the simulations and analysis; D.Z. wrote the draft; and all the authors contributed to the interpretation of the results and writing of the manuscript.

COMPETING INTERESTS

The authors declare no competing interests.

ADDITIONAL INFORMATION

Correspondence and requests for materials should be addressed to Hongxiong Xu or Ying Li.